sustainability

MDPI

Article

Assessing the Effects of Urban Morphology Parameters on Microclimate in Singapore to Control the Urban Heat Island Effect

Hong Jin [1], Peng Cui [1,2,*], Nyuk Hien Wong [2] and Marcel Ignatius [2]

1. School of Architecture, Harbin Institute of Technology, Heilongjiang Cold Region Architectural Science Key Laboratory, No. 66 Xidazhi Street, Nangang District, Harbin 15001, China; jinhong@hit.edu.cn
2. Department of Building, National University of Singapore, School of Design and Environment, 4 Architecture Drive, Singapore 117566, Singapore; bdgwnh@nus.edu.sg (N.H.W.); m.ignatius@nus.edu.sg (M.I.)

* Correspondence: 14b334004@hit.edu.cn; Tel.: +86-451-8628-1155

Received: 25 December 2017; Accepted: 11 January 2018; Published: 16 January 2018

Abstract: It is important to alleviate the "heat island effect" in urban areas, especially tropical cities. Microclimate is normally affected by the urban morphology parameters. The objective of this work is to investigate the correlation between air temperature variations and urban morphology parameters in tropical cities. Field measurement was carried out to record the air temperature at 27 points within an 8 km^2 urban area continuously in Singapore for one year. Geographical information system was applied to extract the urban morphology parameters. Generally, the maximum and minimum air temperature spatial differences in the study area ranged from 3.2 to 6.5 °C, indicating the significant effects of urban morphology on the air temperatures. Based on the fitting results of created multilinear regression models, parametric study has been performed to investigate the specific effects of urban morphology parameters on air temperatures. This work has proposed a much more precise regression model to predict the air temperature with various urban morphology parameters. In addition, meaningful value of reference has been offered for urban planners and landscape designers to effectively control the air temperature in tropical cities such as Singapore.

Keywords: urban heat island effect; air temperature; microclimate; urban morphology parameters tropical city

1. Introduction

The urban heat island (UHI) effect is one of the most severe problem in tropical cities. As the population grows, building density also increases resulting in distinctive surface energy balance and microclimatic characteristics at the local scale [1,2]. The local climate of an urban area may be substantially affected by landscape factors as well as geometrical characteristics, anthropogenic activities, and heat sources present in the area. The urban environment continually shapes the microclimate in numerous ways [3]. There is a mounting research interest in microclimate issues, as they represent important factors in achieving sustainability inside cities, which serve increasingly large populations across the globe. The urban microclimate both influences and is influenced by human behavior and decision-making, due to the complex interactions between air temperature, relative humidity, wind speed, and micro-scale landscape parameters [4–6]. Empirical knowledge of local air temperature variability and the relationship between the microclimate and artificial impact factors is critical in adapting the urban climate to changes in its thermal environment.

Outdoor spaces are important parts of any urban area as they provide thoroughfares for pedestrian traffic as well as venues for outdoor activities. Increased outdoor activity in urbanized areas has a wealth of positive effects on the population. Outdoor spaces must be properly designed for maximum benefit to the urban dwellers who enjoy them. The outdoor microclimate is an important factor in the quality of an urban outdoor space, as it affects thermal comfort throughout all aspects of outdoor activities.

The microclimate is influenced by many factors. As reported within a 50-m radius, critical parameters with significant influence on the minimum temperature (T_{min}) and average temperature (T_{avg}) values include the green plot ratio (*GnPR*), total tree leaf area (*TREE*), and percentage of green area (GREEN); parameters with significant influence on the maximum temperature (T_{max}) are sky view factor (*SVF*), *GnPR*, *TREE*, and *GREEN* [7]. Parks have significant cooling effect upon nearby buildings, and the distance from the nearest park can affect the ambient temperature in a given area [8–10]. As the cooling effects of vegetation or water extend into the surroundings, a park can reduce the air temperature in a busy commercial area by up to 1.5 °C [11].

Urban geometry and the thermal properties of urban surfaces are also important parameters influencing the urban climate [12–15]. The local urban context is made up of buildings, roads, trees, and lawns; land cover features represent various ratios of buildings and vegetated areas. Sun [16] found that air temperature is significantly correlated with green ratio and building ratio during night hours in Taiwan. Yan et al. [17] reported that increasing the percentage of vegetation cover can significantly decrease air temperature, while increase in building area significantly increases air temperature according to field measurements taken in Beijing. Yokobori [18] found that air temperatures vary significantly according to ambient land cover types; air temperatures decrease as the amount of vegetated area around various measurement sites in Japan increase. Sky view factor (*SVF*) is another crucial factor affecting mean radiant temperature (T_{mrt}) which can change with site geometry. When an urban space has high *SVF* condition, it means more solar radiation reaches the ground below during the daytime. The opposite phenomenon occurs at night, forming an "urban cool island". Interestingly, however, some studies have shown that *SVF* has very little impact on air temperature [19,20].

Urban microclimates are a formed via a highly dynamic and complex process which varies within different macroclimate. In addition, due to the differences registered in the thermal perception of different populations, it is necessity to perform study aimed at evaluating the microclimate of a specific city or site [21,22]. According to previous studies, the main microclimate parameters affecting any open space include land cover, site geometry, and spatial location (e.g., proximity to parks or water bodies). Previous researchers have simulated and conducted field measurement on these parameters extensively, but most studies center around single-parameter models—researchers tend to examine one problem from different respective angles corresponding to different respective landscape parameters, which makes it very difficult to conclude which particular landscape factor most significantly affects air temperature within the urban context. In addition, urban climates are affected by external factors such as the topographic features, season, and prevailing weather. It is important to control for geographical, seasonal, and meteorological (e.g., wind speed and cloud cover) variables as much as possible to determine the location-specific changes in urban air temperature.

The purpose of this study can be summarized as follows.

(1) Continuous field measurement at 27 points in the studied area to collect the microclimatic weather conditions at 2.5-m height for one year to investigate the spatial and temporal microclimate parameters related to the distribution of open space at the local scale in Singapore, and explain changes in microclimate within this specific morphology.
(2) Determine the relationship between urban morphology parameters and microclimate parameters, as well as the influence radius of the surrounding urban morphology parameters.
(3) Develop empirical models to correlate the air temperature at 2.5-m height with the urban morphology parameters and weather parameters.

2. Methodology

2.1. Study Area

The Köppen Climate Classification subtype for Singapore climate is "Af" (Tropical Rainforest Climate). Near-surface air temperature usually ranges from 23 °C to 32 °C. April and May are the hottest months, and the monsoon season extends from November to March [23]. The mean annual trends of climate has been summarized in Table 1.

Table 1. The mean annual trends of air temperature, relative humidity and wind speed.

Time Period	Average Temperature (°C)	Average Number of Rainy Days	Average Morning Relative Humidity (%)	Average Evening Relative Humidity (%)	Average Wind Speed (km/h)
ANNUAL	27	218	91	74	12
JAN	27	18	92	74	17
FEB	27	10	92	69	16
MAR	28	15	92	72	14
APR	28	18	93	74	9
MAY	28	20	92	76	9
JUN	28	17	90	72	9
JUL	28	19	90	73	9
AUG	27	17	89	73	12
SEP	27	19	92	75	9
OCT	27	19	92	73	8
NOV	27	24	92	77	6
DEC	26	22	93	8012	8

Singapore is a garden community with no distinct border lines between urban and rural areas. Its street canyon layout differs from other cities in regards to its distinctive landscape elements [24]. We took field measurements in the Jurong Lake area (Figure 1) to establish a working understanding of how the landscape factors impact the ambient environment in Singapore. Jurong East is a residential town representative of the traditional Singaporean street canyon layout. We selected 27 different measurement sites across the study area to ensure a sufficiently wide range of *SVF*s, building plot ratios, and vegetation cover rates in investigating the quantitative relationship between microclimate parameters and landscape (Figure 2). The research area is very flat, so any temperature difference due to topography was negligible. The measurement sites located are sufficiently close to one another to be affected by uniform meso-scale climate conditions, yet also affected by distinctly different micro-scale landscape characteristics.

Figure 1. Location of the study area and measurement sites.

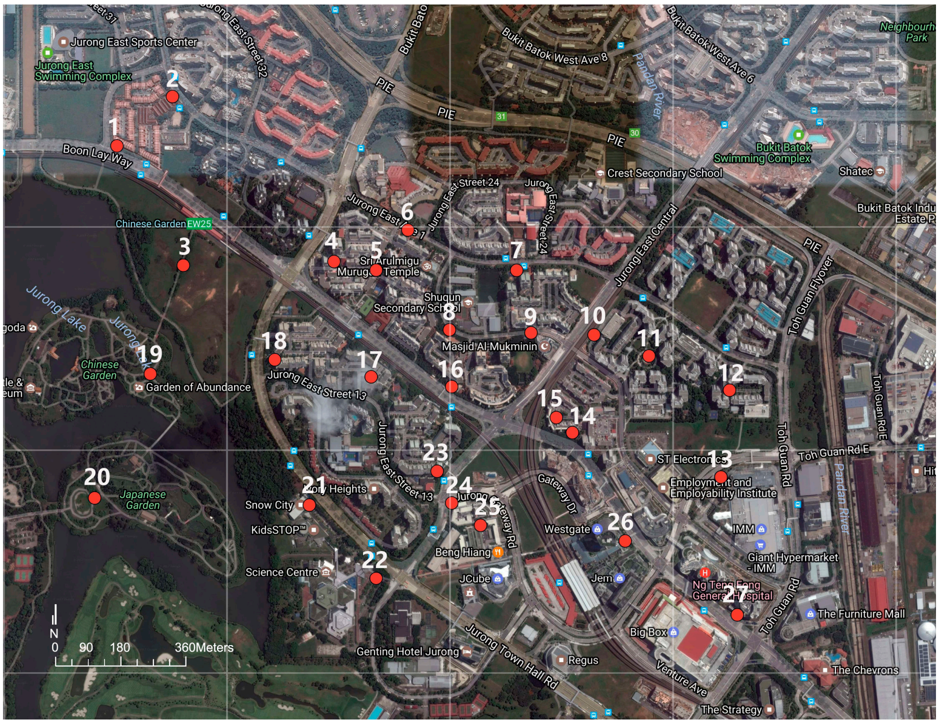

Figure 2. Map view of fixed test points.

2.2. Microclimate Parameter Measurements

Mobile traverse measurements may be affected by error during the test process. It may be challenging to secure sufficient data for real environment microclimate parameter analysis due to such error. We used fixed rather than mobile microclimate stations to conduct measurements from August 2016 to June 2017. Each microclimate station was assembled as shown in Figure 3; the precision of each sensor is listed in Table 2. The steel beam direction was set from west to east to obtain accurate wind direction information. Records were taken in 5 min intervals. Every two weeks, we downloaded the data and changed the sensor batteries. We manually recorded windy, rainy, and cloudy conditions from the ground to investigate different factors influencing the UHI.

Figure 3. Weather station structure.

Table 2. Technical characteristics of measurement instruments.

Temperature/RH	HOBO UX100-014M	
	Global temperature (T_g) ONSET HOBO U23-001 Temperature range/accuracy RH measurement range/accuracy	−40 °C to 70 °C, ± 0.18 °C −40 °C to 70 °C, ±0.2 °C 0–100%, ±2.5%
Wind speed/direction	ONSET S-WSET-A Wind speed & direction sensor	
	Wind direction range Wind speed range/accuracy	2-Axis ultrasonic wind sensor 0–45 m/s (0–100 mph) ±1.1 m/s (2.4 mph)
Data logger	HOBO Micro station logger H21-002	−25 °C to 65 °C
Sky view factor (*SVF*)	Nikon D80 Digital SLR camera with fish eye lens	

2.3. Weather Data Selection for Analysis

The data obtained including air temperature, humidity and wind speed is authentic when the weather conditions are clear and sunny. Therefore, during the measuring period rainy and cloudy days were excluded while clear and sunny days are selected for data analysis and model development. The criterion requiring bell-shaped hourly solar radiation and air temperature profiles was proposed to select analyzed days.

- Daily maximum solar radiation larger than 900 W/m^2;
- Hourly temperature and hourly solar radiation take on a bell shape profile;
- Daily average temperature higher than 24 °C; and
- Daily average wind speed less than 3 m/s.

According to the criterion described above, 50 typical days have been selected. The selected days have been randomly divided into two groups, which were used for model development and validation, respectively. As shown in Table 3, 40 days were selected for model development and 10 days were selected for the validation.

Table 3. Selected date for model development and validation.

40 Days for Model Development		10 Days for Model Validation	
February 2017	2, 8, 9, 25	February 2017	3, 10,26
March 2017	5, 7, 8, 16	April 2017	6, 10, 15
April 2017	2, 5, 6, 10, 13	July 2017	4, 15
May 2017	25, 26, 27	August 2017	18, 21
June 2017	6, 8, 11, 13, 15, 25, 27	September 2017	18, 20
July 2017	1, 3, 5, 6, 10, 18, 21		
August 2017	17, 22, 23, 25, 26, 27		
September 2017	5, 7, 8, 16		
October 2017	1, 6, 10, 18		

2.4. Urban Morphology Parameter Measurement and Computation

Numerous parameters are available to assess and quantify the effects of urban environment characteristics on air temperature [25–28]. However, the Singapore island temperature pattern shows urban heat island characteristics based on the conditions of surrounding buildings, greenery, and pavement [29]. We selected parameters under four main principles: (1) they have potential effects on microclimate; (2) they are easily calculated; (3) they are easily controlled by design; and (4) they have minimal redundancy. In this study, we selected three categories of urban morphology parameters including land cover features, site geometry, and spatial location to measure site environmental characteristics. The land cover features include green plot ratio (*GnPR*), building plot ratio (*BPR*), percentage of pavement (*PP*). (The "plot ratio" is the ratio of the total floor area to the total selected land area.) The site geometry includes sky view factor (*SVF*) and the spatial location include distance to park (*DP*) and distance to water (*DW*). Site geometry was measured using *SVF* and spatial location was measured according to distance to the nearest park and water body. Our main analysis tool in developing the climatic maps was the Geographical Information System (GIS), a technology to view and analyze data from a geographic perspective. GIS links the location and information layers to reveal how they interrelate. The variation in air temperature with regard to the land cover composition of each measurement site was quantified after establishing a buffer zone with 20 m, 50 m, or 70 m radius in this study.

We controlled the variables to fully ensure that every test point provided meaningful information. We used two different *SVF* calculation methods. For 20 m radius, we used an 8mm circular fisheye lens to obtain images which were imported to the Rayman model [30]; for 50 m and 70 m radii, we used GIS (ESRI, Redlands, CA, USA) [31] to obtain the calculations shown in Figure 5g. The effects of parks and water bodies were estimated based on the straight distance between each measurement site and the edge of the park or water body nearest to the site.

The mean radiant temperature is one of the meteorological parameters that can influence human energy balance and human thermal comfort [32]. The global temperature represents the weighted average of radiant and ambient temperatures. If the global temperature, air temperature, and air velocity are known, then T_{mrt} can be calculated according to Equation (1) [33]:

$$T_{mrt} = \left[\left(T_g + 273 \right)^4 + \frac{1.10 \times 10^8 {V_a}^{0.6}}{\varepsilon D^{0.4}} \left(T_g - T_a \right) \right]^{\frac{1}{4}} - 273 \quad (1)$$

where:

T_g = Globe temperature (°C)
V_a = Air velocity (m/s)
T_a = Air temperature (°C)
D = Globe diameter (mm)
ε = Globe emissivity

We performed greenery mapping using the Green Plot Ratio (*GnPR*) method, as developed by Ong (2003). *GnPR* is derived from the average amount of greenery on a given lot per the leaf area index (LAI) in proportion to the total lot area. It is the sum of the products of the area of each greenery type and its corresponding LAI value, which is divided by the total lot area. The *GnPR* equation is as follows [34]:

$$\mathrm{G}nPR = \sum \left(n_n A_n \times LAI_n \right) / Site\ Area \quad (2)$$

where:

LAIn: leaf area index of species *n*
An: canopy area of species *n*
nn: number of plants of species *n* on the site

The values of *DP* and *DW* were obtained by GIS. The description of each test point is shown in Table 4.

Table 4. Description of measuring sites (50 m).

No	*SVF*	*BPR*	*GnPR*	*PP* (%)	*DP* (m)	*DW* (m)	Temp. (°C)	RH (%)	T_{mrt} (°C)	Description of Measurement Sites
1	0.76	1	1.06	70	506	188	30.77	72.88	31.71	Broad street, multi-story buildings
2	0.57	0.35	1.06	63.6	757	397	29.76	77.24	30.32	Broad street, multi-story buildings

Table 4. *Cont.*

No	*SVF*	*BPR*	*GnPR*	*PP* (%)	*DP* (m)	*DW* (m)	Temp. (°C)	RH (%)	T_{mrt} (°C)	Description of Measurement Sites
3	0.38	0	1.25	8.5	238	150	29.16	79.76	29.75	Park's perimeter road, tree cover
4	0.62	1.86	0.20	51.2	769	458	30.01	75.01	30.52	High-rise buildings without trees
5	0.48	5.72	3.24	50	919	606	29.59	79.09	29.77	Broad street, high-rise buildings
6	0.51	2.28	0.62	47.2	714	1028	30.04	77.18	30.06	Broad street, open space
7	0.32	4.3	0.41	31.2	1256	1112	28.94	81.45	29.28	High-rise buildings, tree cover
8	0.51	0.08	0.43	30.4	767	958	29.79	78.75	30.25	High-rise buildings, tree cover
9	0.34	5.7	1.64	28.1	1124	1195	29.09	81.17	29.68	Broad street, multi-story buildings
10	0.52	3.2	2.95	51.4	1229	1410	29.51	80.24	30.2	Broad street, multi-story buildings
11	0.46	2.4	1.0	19.7	1453	1539	29.19	84.56	30.4	Open area with lawn
12	0.32	3.7	1.55	9.6	1521	1778	29.43	79.76	31.44	Broad street, multi-story buildings
13	0.68	0.8	1.89	63.1	1455	1751	30.01	73.46	31.41	Shopping mall without tree
14	0.55	1.05	0.16	31.7	1020	1325	30.21	76.50	30.02	Multi-story buildings, tree cover
15	0.48	2.42	0.41	50.8	937	1254	29.24	80.41	30.01	Multi-story buildings, tree cover
16	0.61	1.9	2.59	31.8	695	994	29.41	81.26	30.03	Open area with few tree
17	0.51	1.8	3.85	21.3	505	791	29.43	75.11	30.01	Multi-story buildings, tree cover
18	0.37	5.4	3.43	29.4	224	520	28.99	83.51	29.38	Broad street, multi-story buildings
19	0.66	0.1	0.49	34.2	122	150	30.39	78.90	30.11	Open area with lawn
20	0.82	0	0.17	33	185	10	30.87	75.03	31.12	Inside the park, open area with lawn
21	0.41	0.37	3.0	47.4	148	514	29.64	77.13	30.25	Open area, parking lot
22	0.44	0.22	0.58	30.8	289	443	29.51	76.96	30.44	Open area, parking lot, tree cover
23	0.54	1.05	1.97	20.7	569	882	29.69	75.57	30.45	High-rise buildings, tree cover
24	0.72	1.17	2.78	61.9	579	883	29.89	78.21	31	Open area without tree
25	0.59	1.57	0.69	30.1	630	980	29.89	78.21	30.95	Multi-story buildings without tree
26	0.51	0.9	1.29	40.8	1011	1406	29.81	75.33	30.1	Open area with tree
27	0.33	0.9	4.37	42.9	1351	1774	29.59	74.87	29.67	Open area with tree

Abbreviations: *SVF*, sky view factor; *BPR*, building plot ratio; *GnPR*, green plot ratio; *PP*, percentage of pavement; *DP*, distance to park; *DW*, distance to water body.

2.5. Regression Analysis for Model Development

Multiple regression analysis was carried out to determine how well the observed air temperature differences could be explained by the combination of the six urban morphology variables (Table 4). The regression results offer insight into the influence of different variables on air temperature at different points in time. The coefficient of determination (R^2) represents the proportion of the variation in air temperature that could be explained by the regression models; the standardized coefficients (Beta coefficients) of predictive models represent the relative contributions of different landscape variables to the air temperature difference. The calculation radius has a strong influence on *BPR*, *GnPR*, and *PP*; different areas have different influence radii [35].

In a similar study on Curitiba, Kruger found that 56 m of the calculation radius had the most significant impact on temperature variation among 56 m, 125 m, and 565 m radii [36]. In Beijing, Yan found that 75 m is the most significant radius [17]. The most significant radius in Singapore remains unclear, so we chose three radii to test the calculation impact on urban microclimate by comparison.

We used a multivariate regression analysis to quantify the relative contribution of six landscape variables to differences in air temperature. The predictive model is:

$$Y = a + b_1 BPR + b_2 GnPR + b_3 SVF + b_4 DP + b_5 DW + b_6 PP$$

3. Results and Analysis

3.1. Correlation between Air Temperature and Urban Morphology Parameters

Table 5 shows the significance of six urban morphology parameters with three calculation radii. During daytime hours, 83.2% of the air temperature data could be accurately predicted by the six parameters when the calculation radius is 20 m, 91.7% for 50 m and 87.4% for 70 m, respectively, According to the R^2 values, the 50-m radius has the most significant impact on temperature variation in Singapore. The Beta coefficients indicated that among all six parameters, *SVF* is the most significant parameter. According to this model, 10% increase of *SVF* would lead to an increase of air temperature by 0.21 °C when the radius is 50 m. When calculation radius becomes wider, *BPR* becomes another important impact factor; the air temperature decreased by 0.13 °C when *BPR* increased to 10%. The negative coefficients of *GnPR* and *BPR* suggest that an increase in green plot ratio and building plot ratio would decrease the air temperature. By contrast, the positive coefficients of *SVF*, *DP*, and *DW* altogether indicate that temperature would increase with increased distance from parks or water bodies, although which significances are relatively smaller.

The six urban variables can explain the daytime temperature variables much better than nighttime. During nighttime hours, 67% of the air temperature data could be accurately predicted by the six parameters when the calculation radius is 20 m, 67.7% for 50 m and 64.2% for 70 m, respectively. *SVF* is the most significant parameter for all calculation radius. A 10% increase in *SVF* decreased air temperature by 0.14 °C, 0.17 °C, and 0.08 °C respective to the three radii we tested. The negative coefficients of *GnPR* and *SVF* suggest that an increase in green plot ratio or *SVF* would decrease air temperature. By contrast, the positive coefficients of *DP* and *DW* indicate that temperature would increase with increasing distance from parks or water bodies.

Based on the measured data on selected days listed in Table 3, Equations (2)–(6) were developed to predict $T_{avg\text{-}day}$, $T_{avg\text{-}night}$, T_{avg}, T_{max} and T_{min}, respectively. Equations (2) and (3) show that T_{avg} is correlated to daytime and night average temperature at meteorological station (Ref $T_{avg\text{-}day}$), the minimum relative humidity (RH_{min}) and average wind speed ($WIND_{avg}$).

$$T_{avg\text{-}day} = 2.31 + 0.778 RefT_{avg\text{-}day} - 0.11 RH_{min}(\%) - 0.341 WIND_{avg} \quad (R^2 = 98.7,\ F = 9815.39,\ Standard\ Error = 0.51) \tag{3}$$

$$T_{avg\text{-}night} = 0.57 + 1.11 RefT_{avg\text{-}day} - 0.67 RH_{min}(\%) - 0.228 WIND_{avg} \quad (R^2 = 92.1,\ F = 9134.51,\ Standard\ Error = 0.55) \tag{4}$$

Equations (5) and (6) show the relationship between the air temperature and urban morphology parameters. T_{max} appears during daytime and T_{min} appears during nighttime.

$$T_{max} = 2.97 SVF - 0.003 GnPR - 0.019 BPR - 1.13\text{E-}5 DP - 1.112\text{E-}5 DW + 1.76 PP + 28.57 \quad (R^2 = 91.7,\ F = 8814.31,\ Standard\ Error = 0.322) \tag{5}$$

$$T_{min} = -0.706SVF - 0.014GnPR + 0.026BPR - 2.45\text{E-}5DP + 0.6\text{E-}5DW + 0.026PP + 28.894 \quad (R^2 = 77.7, F = 12991.11, Standard\ Error = 0.33) \tag{6}$$

Equations (3)–(6) were validated against the measured temperatures, as listed in Table 3. Figure 4 has illustrated the deviations between the predicted and measured $T_{avg\text{-}day}$, $T_{avg\text{-}night}$, T_{avg}, T_{max} and T_{min}, respectively. In the box plot, the black line in the middle of box is the median temperature difference values. The bottom and top of box indicate the 25 and 75 percentage, respectively. The values between the five predicted and measured temperatures are all close to 0 °C. Overall, 96% of the values fell in the range of −1 °C to 1 °C (region of shallow green), while 54% of fell in the range of −0.5 °C to 0.5 °C (region of dark green). In addition, the accuracies of these estimations were evaluated by the index of normalized root mean square error ($NRMSE$) using Equation (7), which is defined as the ratio between the root mean square error $RMSE_i$ (calculated from predicted temperature) and $RMSE_{i=ref}$ (calculated considering that each station is at the reference temperature value) [37].

$$NRMSE = \frac{RMSE_i}{RMSE_{i=ref}} = \sqrt{\frac{\sum_1^{Nd}\sum_1^{Ns}\left(T_{mea,i}(j) - T_{est,i}(j)\right)^2}{\sum_1^{Nd}\sum_1^{Ns}\left(T_{mea,i}(j) - T_{ref,i}\right)^2}} \tag{7}$$

Table 5. Regression results of air temperature and six landscape variables. The bold figures are significant variable with $p < 0.05$.

Variables		20 m			50 m			70 m		
		B	Beta	Sig.	B	Beta	Sig.	B	Beta	Sig.
Day-time	*SVF*	2.1	0.58	**0.000**	2.792	0.724	**0.000**	2.338	0.612	0.000
	BPR	−0.75	−0.27	0.439	−0.019	−0.243	0.05	0.011	−0.255	0.055
	GnPR	−0.004	−0.18	0.052	−0.003	−0.51	0.333	−0.007	−0.46	0.137
	PP	0.04	0.125	0.410	1.76	0.21	0.444	1.47	0.133	0.468
	DP	0.000	−0.03	0.905	−0.000	0.113	0.127	−0.000	−0.099	0.388
	DW	0.000	−0.182	0.470	0.000	−0.091	0.929	0.000	−0.082	0.778
	Constant		28.90			28.57			29.44	
	R^2		0.832			0.917			0.874	
	Adjusted R^2		0.795			0.863			0.771	
Night-time	*SVF*	−0.664	0.276	0.139	−0.706	−0.293	0.131	−0.733	−0.293	0.147
	BPR	0.039	0.208	0.305	0.026	0.132	0.472	0.026	0.147	0.412
	GnPR	−0.015	−0.332	**0.041**	−0.014	−0.306	**0.047**	−0.027	−0.333	0.050
	PP	0.003	0.141	0.512	0.026	0.132	0.239	0.026	0.139	0.331
	DP	0.000	−0.197	0.589	0.000	−0.245	0.507	0.000	−0.211	0.557
	DW	0.000	0.530	0.139	0.000	0.605	0.107	0.000	0.555	0.122
	Constant		29.026			28.894			27.97	
	R^2		0.670			0.777			0.642	
	Adjusted R^2		0.615			0.629			0.607	

Abbreviations: B, unstandardized coefficient; Beta, standardized coefficient; and Sig., significant level. Note: This research set 0.05 as the threshold and significance indicates that, when p value < 0.05, the variables can effectively explain the change of temperature. Note: the figures in bold are significant variable with $p < 0.05$.

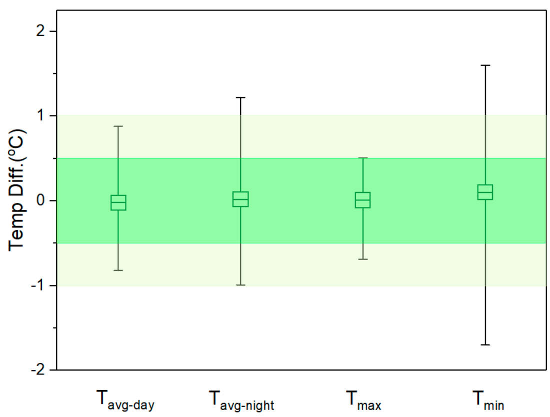

Figure 4. Time deviations between predicted and detected temperatures.

3.2. Influence of Temporal and Spatial Variation on Microclimate

Figure 5 shows the changes in temperature and RH as time during the whole day period for each measuring point. The spatial patterns of the microclimate parameters are shown in Figure 6. In addition, the daytime data in Figure are the average data at 14:00, while the nighttime data are at 02:00 from clear days in June, July and August 2017. Figure 5 also shows where the air temperature and RH differences among different locations were very significant. During the day, the max air temperature difference between the lowest Point (12) and highest Point (19) at the same time reached up to 6.5 °C. RH differed by 15% between the lowest Point (20) and highest Point (12).

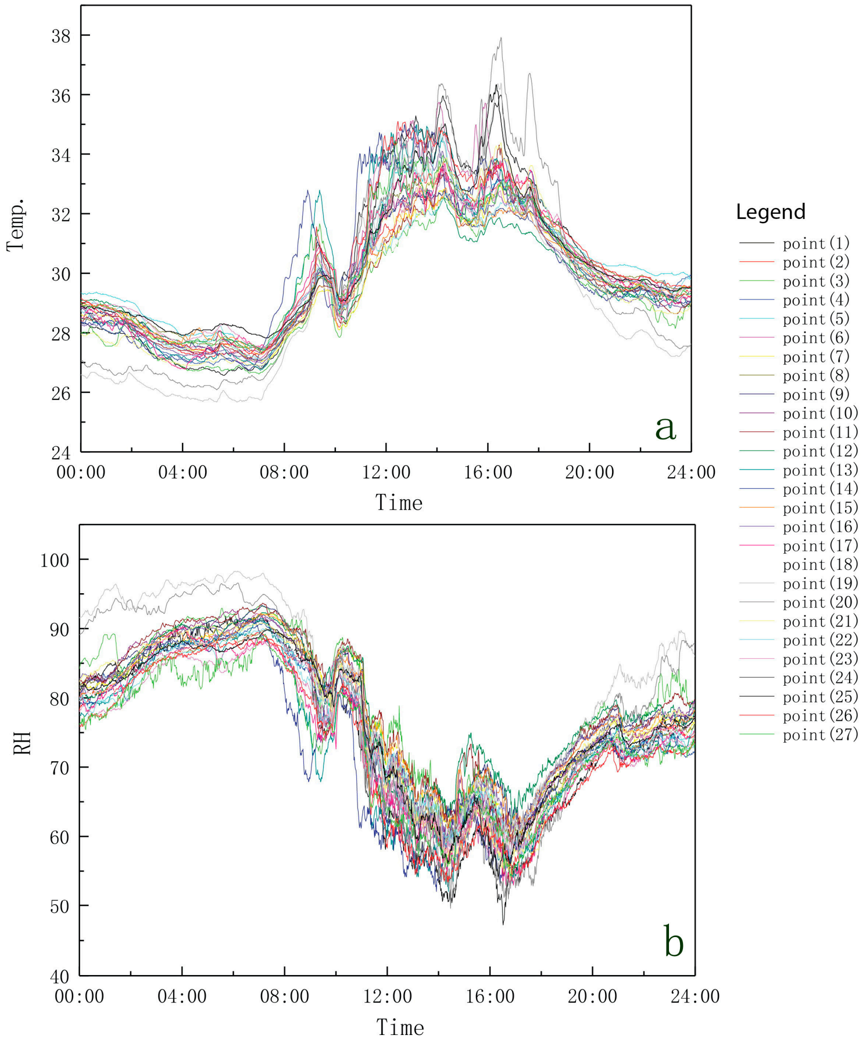

Figure 5. Profiles of (**a**) air temperature and (**b**) RH from 0:00 UTC to 24:00 UTC for all testing points.

The trends for temperature rose sharply at every test point with time from 08:00 to 14:00, then fell to a smooth interval until 08:00 the following day. The hottest place was at Point (20), which had mean air temperature of 37.2 °C. This site is located in an open space with grass cover but without any shading and is fully exposed to solar radiation during the day. Though the transpiration of greenery can reduce air temperature, shading is a much more important factor in tropical cities. The lowest temperature appeared on Point (7), which has the lowest *SVF*. As shown in Figure 6a, the test points with lower temperatures are all located in the center of the commercial area despite the high anthropogenic heat flux also present in this area. The shading from trees and high plot ratio of buildings appears to stave off the continuous heating of the pavement surface by solar radiation.

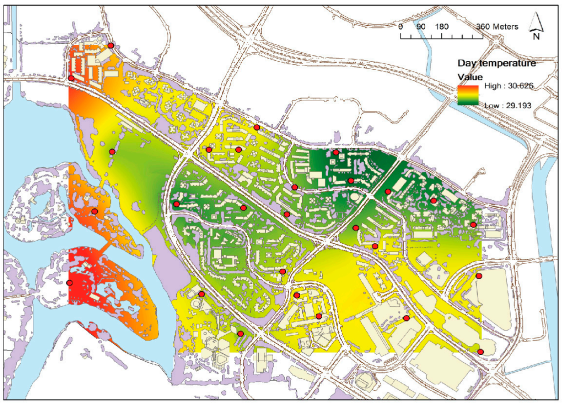

(a) Temperature distribution during daytime

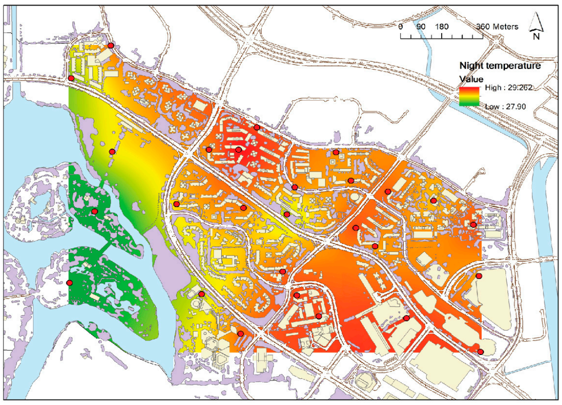

(b) Temperature distribution during nighttime

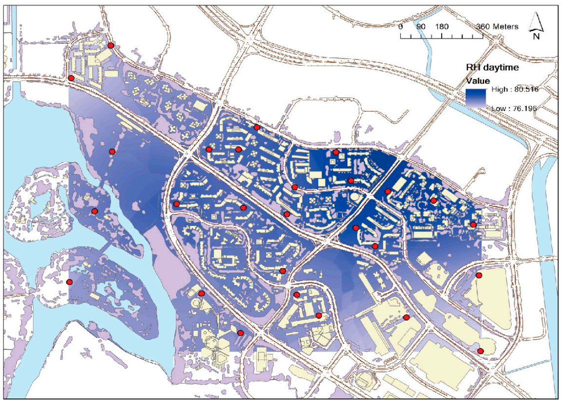

(c) RH distribution during daytime

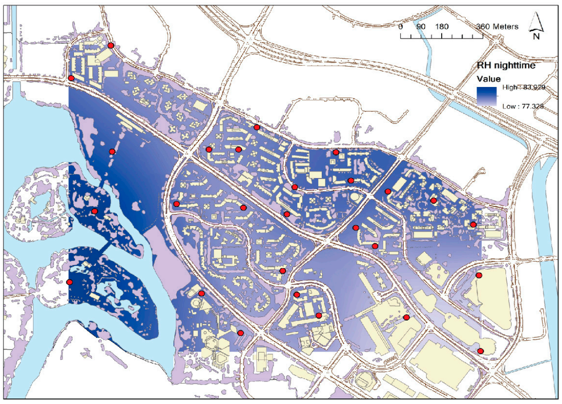

(d) RH distribution during nighttime

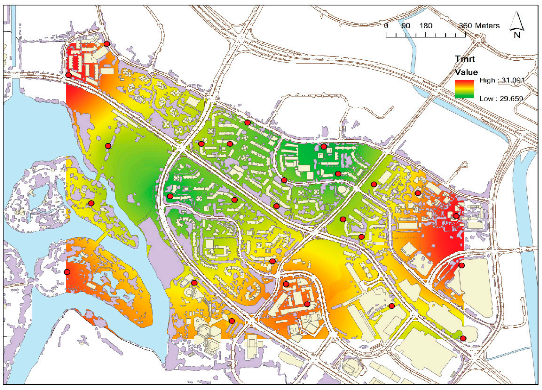

(e) Tmrt distribution

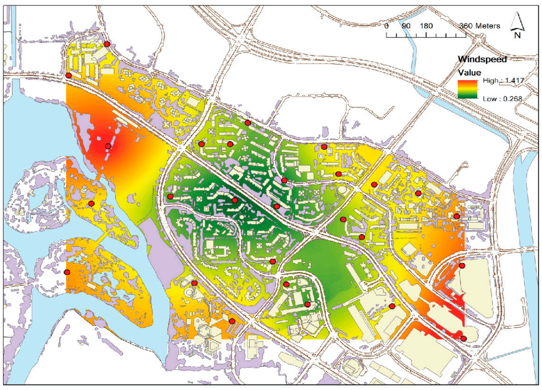

(f) Wind speed distribution

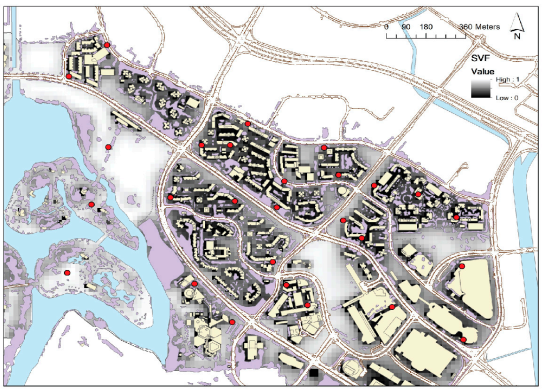

(g) SVF distribution

Figure 6. Mapping of the microclimate parameters.

The distribution of T_{mrt} is slightly different from the temperature distribution due to the differing albedo among different interfaces (Figure 6e). Besides, T_{mrt} increases as *SVF*, which is discussed in detail in the following section. The distribution of T_{mrt} has a significant correlation with *SVF* (Figure 6g). During the daytime, RH increases slightly with *DW*, however, not significantly. The RH distribution during the nighttime period is opposite to that during the daytime period (Figure 6c,d). The RH near water was also higher than in other areas throughout the study period (Figure 6d). In the building area, the RH is almost uniform. During nighttime, the temperature distribution pattern in the study area becomes especially clear (Figure 6b). The park areas are transformed into cool islands surrounded by hot areas. The mean air temperature difference between the lowest point inside the park and the highest point in the building area reached 4.3 °C. The high *BPR* and low *SVF* make heat less easily dissipated by winds moving through the area (Figure 6f).

3.3. Influence of Site Geometry Parameter on Microclimate

SVF is the most important factor impacting air temperature in tropical cities as previous report [38]. During the daytime, air temperatures in our study area increased with increasing *SVF* (Figure 7a). Less "sky openness" resulted in lower air temperatures under the effects of solar radiation. According to the statistical measurements we obtained, about 59% ($p < 0.001$) of the open space variations in air temperature can be explained by the variations in *SVF* during the daytime. Conversely, this correlation was negative during nighttime hours—at night, the net outgoing long-wave decreased at locations with low *SVF* values, resulting in higher temperatures (Figure 7b). *SVF* also can explain 15% of air temperature variation during the night.

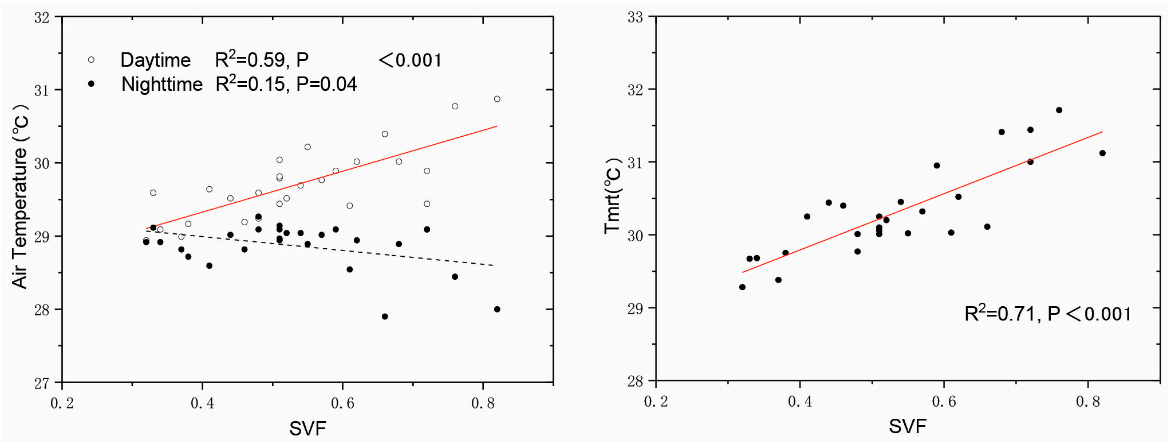

(a)Relationships between air temperature and SVF
(b)Relationships between Tmrt and SVF

Figure 7. Relationships between microclimate parameters and *SVF* during day and night with the radius of 50 m.

Open space with less vegetation has a very high daytime air temperature due to the maximum solar heat gain received by the ground surface. Air temperature is quite cooler at night because the heat is released to the atmosphere without any entrapment by the surrounding buildings. On the contrary, sites dense with buildings and surrounded by little vegetation, heat accumulates during the day due to the lack of greenery but is not easily released due to the heat capacity of the surrounding buildings.

Vegetation reduces the sky openness in an urban environment. During the day, we observed a significant and close correlation between *SVF* and air temperature ($R^2 = 0.59$, $p < 0.001$). In general, higher *SVF* yields higher air temperature. Larger open areas receive more solar radiation, which leads to a higher air temperature. Trees reduce the level of sky openness (i.e., provide shading), thus, they cool the air temperature. At night, we observed a weak correlation between *SVF* and air temperature ($R^2 = 0.15$, $p = 0.04$). There is no adverse impact (i.e., reduction of nighttime net long-wave loss) due to the reduction of *SVF* by trees in the study area.

3.4. Influence of Land Cover Parameters on Temperature

The 50 m radius best explained the temperature variables, so we focused on this radius in our subsequent analysis of the relationship between the land cover features and microclimate. The land cover composition affects air temperatures differently at different time points, as shown in Figure 8. During daytime hours, there was a negative correlation between air temperature and *BPR* (Figure 8a; $R^2 = 0.31$, $p = 0.002$) but a positive correlation between them at night ($R^2 = 0.13$, $p = 0.06$). When the *BPR* reached 5.6, temperature was balanced due to the corresponding low *SVF*. As indicated by Figure 8b, no obvious correlation exists between wind speed and *BPR*, which is due to that wind speed is rather random and normally associated with the architectural composition as well as vegetation. However, it could be deduced from Equations (3) and (4) that the wind speed has certain correlation with the $T_{avg\text{-}day}$. In Figure 8c, it is shown that vegetation reduced the temperature during daytime hours, or rather each 10% increase in *GnPR* decreased temperature by 0.3 °C (daytime: $R^2 = 0.47$, $p < 0.001$). During nighttime, however, this relationship was less significant (nighttime: $R^2 = 0.18$, $p < 0.017$). Other similar studies in Beijing and Tokyo actually showed phenomena opposite to the ones in this work [17,18]. In terms of vegetation, the LAI index of trees specifically (as opposed to shrubs or grass) provides shading which mitigates the effects of solar radiation; the transpiration of greenery can also reduce air temperature. Within the markedly complex urban context, however, *GnPR* is not the main factor controlling the air temperature. Even with high percentage of vegetation cover, the temperature does not easily change without shading because solar radiation makes the greenery less able to perform transpiration. Plants in Singapore have relatively high LAI index, i.e., better cooling effects than plants in colder regions. As shown in Figure 8d, we also found no significant relationship between RH and *GnPR* in either day or night ($R^2 = 0.05$, $p = 0.21$; $R^2 = 0.02$, $p = 0.71$).

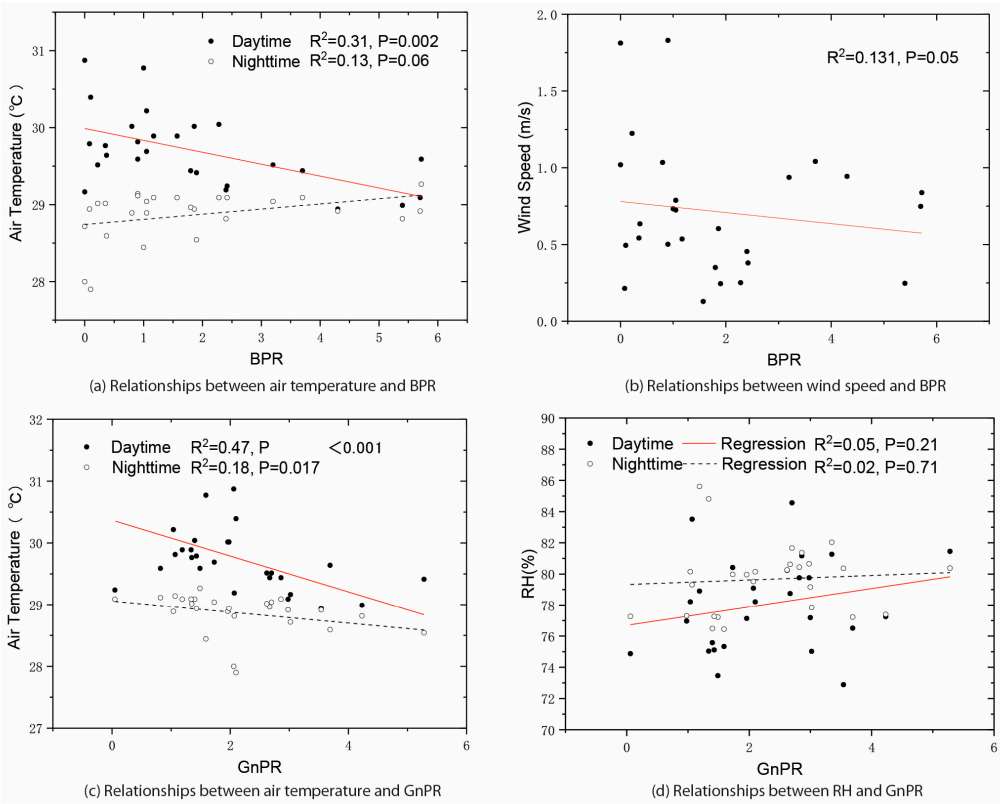

Figure 8. Relationships between microclimate parameters with *BPR* and *GnPR* during day and night with the radius of 50 m.

3.5. Influence of Spatial Location Parameters on Temperature

Figure 9a,c shows the relationships between air temperature with *DP* or water *DW*, respectively. During nighttime hours, air temperature increased with increasing distance to the nearest park, indicating that this variable (distance to park) accounted for 28% of the variance in the air temperature distribution. However, there was no such significant relationship between air temperature and distance to park during the day (R^2 = 0.08, p = 0.13). The air temperatures determined by the distance to water variable were similar: R^2 values were 0.12 and 0.32 during daytime and nighttime, respectively. No significant correlation exists RH and distance to water during the day.

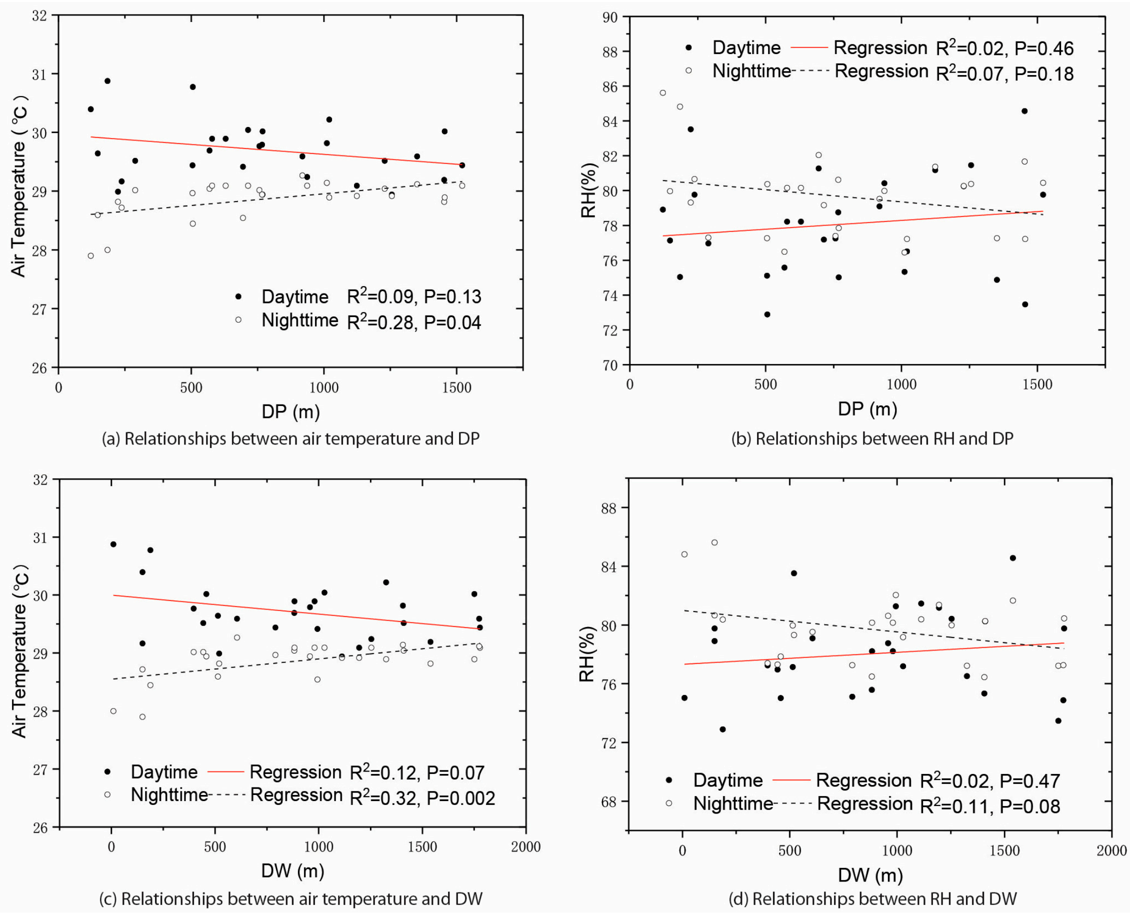

Figure 9. Relationships between microclimate parameters and spatial parameters during day and night with the radius of 50 m.

4. Discussion

Our remote sensing results reflect sizable spatial differences in temperature across the study area. The magnitude and spatial characteristics of these differences varied depending on time of the day. At night, the pattern of temperature distribution in the study area was very clear. Park areas became cool islands surrounded by hotter building areas. The spatial pattern formed in daytime hours tended to be less well-defined. Daytime air temperatures in high-rise building areas were occasionally cooler than those in the park sites, resulting in some urban cool islands. Similar phenomena were observed by Chow and Roth [39], which are attributed to the slower warming of urban surfaces due to the solar heat storage of building materials and the shading effect of nearby buildings and trees.

The maximum air temperature differences between the hottest and coldest sites reached 6.5 °C at day and 3.2 °C at night at the same time in different urban contexts. Air temperature differences were greater, especially during clear and calm weather conditions. This is largely attributable to the difference in radiative cooling rates between natural vegetation and building areas. Mature trees in the form of roadside plantings and plantings between buildings appeared able to provide good shading during the day, but did not provide any noticeable evaporation cooling at night. The long-wave heat release from the surrounding buildings and surfaces was much greater. Thus, areas with similar configuration would also show a relatively cool daytime air temperature and a much warmer nighttime air temperature.

At night, vegetated areas (Points (3), (19), and (20)) were more exposed to the sky than building areas and thus experienced a higher cooling rate. At the same time, the decrease in temperature in the building area was lower because surrounding structures influenced the loss of long-wave radiation to the sky.

To explore the driving mechanisms of air temperature differences varied with times, we analyzed the correlation between daytime air temperature and the nighttime air temperature (Figure 10). The significant correlation between the air temperature in the night time and that in the day time implies that the urban morphology parameters affecting the temperature are the same for the night time and day time. On the contrary, weak correlation indicates that the distinct parameters mainly dominate the temperature in the day time or night time [17]. It can be seen in Figure 10 that the correlation between the temperature in the night time and that in the day time is rather weak ($R^2 = 0.24$, $p = 0.009$), which indicates there exist other parameters affecting the temperature. During the day, the air temperature variations at different locations were influenced by more factors, such as the heat from window air conditioners and traffic. At nighttime, however, the spatial temperature pattern was more complex; air temperature differences may be mainly attributable to the differences in cooling, specifically, among different sites.

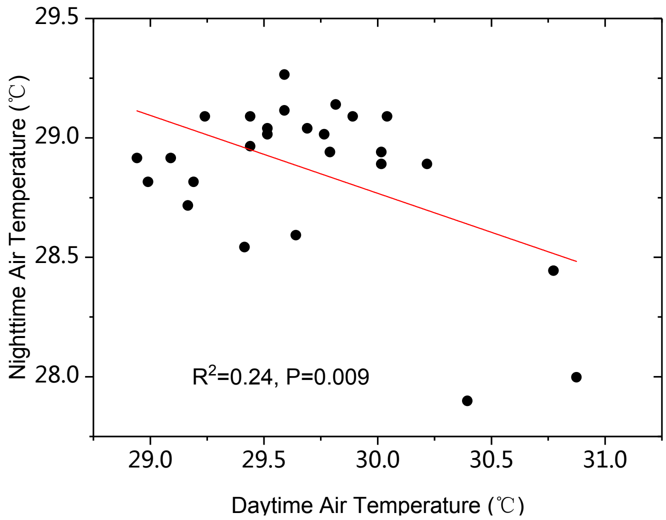

Figure 10. Relationships between daytime temperature and nighttime temperature.

The cooling effect of vegetation was stronger at night than during the day per our standardized coefficients, although said effects varied slightly with calculation radius. This is mainly because vegetation inherently affects air temperature in different ways at different times. During the day, vegetation strongly impacts cooling temperature through partitioning solar radiation into latent heat rather than sensible heat. At daytime, shading from vegetation also produces cooling effect on ambient air temperature. During nighttime, however, the lower air temperature in vegetated areas is mainly due to the elevated radiative cooling rate. Thus, it seems that the cooling effect of vegetation produced by a higher cooling rate in the vegetated area at night could exceed that produced by a combination of evapotranspiration and shading during the day. We also found that an increase in *BPR* also significantly decreased air temperature during the daytime but increased it during the nighttime. The impact of *BPR* is in providing shading during the day and dissipating heat as radiative energy, resulting in a lower daytime temperature and higher nighttime temperature. In a tropical climate, high *BPR* can reduce the speed of winds which would otherwise carry heat away from buildings. Previous studies have indicated that the intra-urban air temperature is also related to urban geometry as-measured by H/W (height/width) ratio or *SVF* [40]. Suitable shading and sufficiently wide wind corridors can both be controlled appropriately by adjusting the H/W ratio.

Air temperature in our study area increased with increasing distance from the nearest park or water body, and more clearly in nighttime than in daytime (Figure 9a,c). In Singapore, Chen and Wong [40] carried out measurements in two large parks to also find that air temperature gradually increases with increasing distance from the park boundary. These results may be indicative of an extension of the park's cooling effect into its surroundings, suggesting that parks modify the urban thermal environment. The relationship between air temperature and distance to water (R^2 = 0.32, p = 0.009) was very similar to the relationship between air temperature and distance to park (R^2 = 0.28, p = 0.002). A combination of two factors likely explains this relationship. First, a water body is moist and cool compared to its surroundings and therefore may impact the microclimate of the neighborhood; parks function similarly. Second, in our study area, there is a water body located in the center of the park so there was a complex cooling effect exerted by both elements.

5. Conclusions

In summary, we have affirmed the comprehensive affecting radius of vital urban morphology parameters, including *SVF*, *BPR*, *GnPR*, *PP*, *DP* and *DW*, on the air temperatures has been affirmed to be 50m during the whole day period in Singapore for the first time. In addition, the most important parameter to affect the daytime air temperature is *BPR* and *SVF*. In the nighttime, *GnPR* was the only significant predictor of air temperature. This work has illustrated the systematic research paradigm to study the urban microclimate. Noteworthy, this work would also offer meaningful value of reference for urban planners and landscape designers to effectively alleviate the hot island effect in tropical cities such as Singapore.

Acknowledgments: The material of study is based on collaborative research project of Development of a Climate Change Information Service (CLICIS)@GeoSpace. The authors wish to thank members of the National Environment Agency for the support of this work. Any opinions, findings, and conclusions or recommendations expressed in this study are those of authors and do not necessarily reflect those of the National Environment Agency.

Author Contributions: P.C., N.H.W. and H.J. conceived and designed the experiments; P.C. performed the experiments; P.C. analyzed the data; N.W. and M.I. contributed reagents/materials/analysis tools; P.C. wrote the paper.

Conflicts of Interest: The authors declare no conflict of interest.

References

1. Oke, T.R. The energetic basis of the urban heat island. *Q. J. R. Meteorol. Soc.* **1982**, *108*, 1–24. [CrossRef]
2. Alavipanah, S.; Wegmann, M.; Qureshi, S.; Weng, Q.; Koellner, T. The role of vegetation in mitigating urban land surface temperatures: A case study of Munich, Germany during the warm season. *Sustainability* **2015**, *7*, 4689–4706. [CrossRef]
3. Santamouris, M. Heat island research in Europe: The state of the art. *Adv. Build. Energy Res.* **2007**, *1*, 123–150. [CrossRef]
4. Jeong, S.Y.; Yoon, S.H. Method to quantify the effect of apartment housing design parameters on outdoor thermal comfort in summer. *Build. Environ.* **2012**, *53*, 150–158. [CrossRef]
5. Eliasson, I. The use of climate knowledge in urban planning. *Landsc. Urban Plan.* **2000**, *48*, 31–44. [CrossRef]
6. Brown, R.D. Ameliorating the effects of climate change: Modifying microclimates through design. *Landsc. Urban Plan.* **2011**, *100*, 372–374. [CrossRef]
7. Jusuf, S.K.; Wong, N.H.; Wong, Z.Y.; Tan, E. Transformation of industrial planning in Singapore: Study on the micro-climatic condition of different industrial estates. *Build. Environ.* **2014**, *80*, 48–60. [CrossRef]

8. Givoni, B. Impact of planted areas on urban environmental quality: A review. *Atmos. Environ. Part B Urban Atmos.* **1991**, *25*, 289–299. [CrossRef]
9. Salata, F.; Golasi, I.; Petitti, D.; de Lieto Vollaro, E.; Coppi, M.; de Lieto Vollaro, A. Relating microclimate, human thermal comfort and health during heat waves: An analysis of heat island mitigation strategies through a case study in an urban outdoor environment. *Sustain. Cities Soc.* **2017**, *30*, 79–96. [CrossRef]
10. Lee, H.; Mayer, H.; Chen, L. Contribution of trees and grasslands to the mitigation of human heat stress in a residential district of Freiburg, Southwest Germany. *Landsc. Urban Plan.* **2016**, *148*, 37–50. [CrossRef]
11. Yu, C.; Hien, W.N. Thermal benefits of city parks. *Energy Build.* **2006**, *38*, 105–120. [CrossRef]
12. Skelhorn, C.; Lindley, S.; Levermore, G. The impact of vegetation types on air and surface temperatures in a temperate city: A fine scale assessment in Manchester, UK. *Landsc. Urban Plan.* **2014**, *121*, 129–140. [CrossRef]
13. Upmanis, H.; Chen, D. Influence of geographical factors and meteorological variables on nocturnal urban park temperature differences a case study of summer 1995 in Göteborg, Sweden. *Clim. Res.* **1999**, *13*, 125–139. [CrossRef]
14. Ca, V.T.; Asaeda, T.; Abu, E.M. Reductions in air conditioning energy caused by a nearby park. *Energy Build.* **1998**, *29*, 83–92. [CrossRef]
15. Oke, T.R.; Johnson, G.T.; Steyn, D.G.; Watson, I.D. Simulation of surface urban heat islands under 'ideal' conditions at night Part 2: Diagnosis of causation. *Bound. Layer Meteorol.* **1991**, *56*, 339–358. [CrossRef]
16. Sun, C.Y. A street thermal environment study in summer by the mobile transect technique. *Theor. Appl. Climatol.* **2011**, *106*, 433–442. [CrossRef]
17. Yan, H.; Fan, S.; Guo, C.; Wu, F.; Zhang, N.; Dong, L. Assessing the effects of landscape design parameters on intra-urban air temperature variability: The case of Beijing, China. *Build. Environ.* **2014**, *76*, 44–53. [CrossRef]
18. Yokobori, T.; Ohta, S. Effect of land cover on air temperatures involved in the development of an intra-urban heat island. *Clim. Res.* **2009**, *39*, 61–73. [CrossRef]
19. Eliasson, I. Urban nocturnal temperatures, street geometry and land use. *Atmos. Environ.* **1996**, *30*, 379–392. [CrossRef]
20. Liang, J.; Gong, J.; Sun, J.; Liu, J. A customizable framework for computing sky view factor from large-scale 3D city models. *Energy Build.* **2017**, *149*, 38–44. [CrossRef]
21. Golasi, I.; Salata, F.; de Lieto Vollaro, E.; Coppi, M.; de Lieto Vollaro, A. Thermal perception in the mediterranean area: Comparing the mediterranean outdoor comfort index (moci) to other outdoor thermal comfort indices. *Energies* **2016**, *9*, 550. [CrossRef]
22. Krüger, E.; Rossi, F.; Drach, P. Calibration of the physiological equivalent temperature index for three different climatic regions. *Int. J. Biometeorol.* **2017**, *61*, 1323–1336. [CrossRef] [PubMed]
23. WEATHER Wise Singapore. National Environment Agency. Available online: http://app2.nea.govsg/data/cmsresource/20090721544571208250.pdf (accessed on 21 July 2009).
24. Wong, N.H.; Yu, C. Study of green areas and urban heat island in a tropical city. *Habitat Int.* **2005**, *29*, 547–558. [CrossRef]
25. Bahi, H.; Rhinane, H.; Bensalmia, A.; Scherer, D. Effects of urbanization and seasonal cycle on the surface urban heat island patterns in the coastal growing cities: A case study of Casablanca, Morocco. *Remote Sens.* **2016**, *8*, 829. [CrossRef]
26. Geletič, J.; Lehnert, M.; Dobrovolný, P. Land Surface Temperature Differences within Local Climate Zones, Based on Two Central European Cities. *Remote Sens.* **2016**, *8*, 788. [CrossRef]
27. Wang, J.; Zhan, Q.; Guo, H. The Morphology, Dynamics and Potential Hotspots of Land Surface Temperature at a Local Scale in Urban Areas. *Remote Sens.* **2015**, *8*, 18. [CrossRef]
28. Sismanidis, P.; Keramitsoglou, I.; Kiranoudis, C.T.; Bechtel, B. Assessing the capability of a downscaled urban land surface temperature time series to reproduce the spatiotemporal features of the original data. *Remote Sens.* **2016**, *8*, 274. [CrossRef]
29. Jusuf, S.K. Development of Estate Level Climate Related Impact Assessment Framework and Air Temperature Prediction within Urban Climatic Mapping Method in Singapore. Ph.D. Thesis, National University of Singapore, Singapore, 2009.
30. Matzarakis, A.; Rutz, F.; Mayer, H. Modelling radiation fluxes in simple and complex environments—Application of the RayMan model. *Int. J. Biometeorol.* **2007**, *51*, 323–334. [CrossRef] [PubMed]

31. Wong, N.H.; Jusuf, S.K.; Tan, C.L. Integrated urban microclimate assessment method as a sustainable urban development and urban design tool. *Landsc. Urban Plan.* **2011**, *100*, 386–389. [CrossRef]
32. American Society of Heating, Refrigerating and Air Conditioning Engineers (ASHRAE). *Handbook A, Fundamentals*; American Society of Heating, Refrigerating and Air Conditioning Engineers: Atlanta, GA, USA, 2001; pp. 99–110. ISBN 0910110565.
33. International Standard Organization (ISO). *ISO 7726, Ergonomics of the Thermal Environment, Instruments for Measuring Physical Quantities*; International Standard Organization: Geneva, Switzerland, 1998; pp. 45–51. ISBN 058038651.
34. Ong, B.L. Green plot ratio: An ecological measure for architecture and urban planning. *Landsc. Urban Plan.* **2003**, *63*, 197–211. [CrossRef]
35. Zakşek, K.; Bechtel, B. Source area estimation of urban air temperatures. *Urban Remote Sens. Event (JURSE)* **2015**, 1–4. [CrossRef]
36. Krüger, E.; Givoni, B. Outdoor measurements and temperature comparisons of seven monitoring stations: Preliminary studies in Curitiba, Brazil. *Build. Environ.* **2007**, *42*, 1685–1698. [CrossRef]
37. Bernard, J.; Musy, M.; Calmet, I.; Bocher, E.; Keravec, P. Urban heat island temporal and spatial variations: Empirical modeling from geographical and meteorological data. *Build. Environ.* **2017**, *125*, 423–438. [CrossRef]
38. Hien, W.N.; Jusuf, S.K. Air temperature distribution and the influence of sky view factor in a green Singapore estate. *J. Urban Plan. Dev.* **2009**, *136*, 261–272. [CrossRef]
39. Chow, W.T.L.; Roth, M. Temporal dynamics of the urban heat island of Singapore. *Int. J. Climatol.* **2006**, *26*, 2243–2260. [CrossRef]
40. Johansson, E. Influence of urban geometry on outdoor thermal comfort in a hot dry climate: A study in Fez, Morocco. *Build. Environ.* **2006**, *41*, 1326–1338. [CrossRef]